



Resonant phase-matching between a light wave and a free-electron wavefunction

Raphael Dahan^{1,2}, Saar Nehemia^{1,2}, Michael Shentcis¹, Ori Reinhardt¹, Yuval Adiv¹, Xihang Shi¹, Orr Be'er¹, Morgan H. Lynch¹, Yaniv Kurman¹, Kangpeng Wang¹ and Ido Kaminer¹  

Quantum light-matter interactions of bound electron systems have been studied extensively. By contrast, quantum interactions of free electrons with light have only become accessible in recent years, following the discovery of photon-induced near-field electron microscopy (PINEM). So far, the fundamental free electron-light interaction in all PINEM experiments has remained weak due to its localized near-field nature, which imposes an energy-momentum mismatch between electrons and light. Here, we demonstrate a strong interaction between free-electron waves and light waves, resulting from precise energy-momentum phase-matching with the extended propagating light field. By exchanging hundreds of photons with the field, each electron simultaneously accelerates and decelerates in a coherent manner. Consequently, each electron's quantum wavefunction evolves into a quantized energy comb, spanning a bandwidth of over 1,700 eV, requiring us to extend the PINEM theory. Our observation of coherent electron phase-matching with a propagating wave is a type of inverse-Cherenkov interaction that occurs with a quantum electron wavefunction, demonstrating how the extended nature of the electron wavefunction can alter stimulated electron-light interactions.

The interaction between free electrons and light lies at the core of quantum electrodynamics and has been instrumental in a wide range of applications throughout the years. The development of photon-induced near-field electron microscopy (PINEM) in 2009¹ and its theoretical quantum description in 2010^{2,3} opened the door for numerous experimental and theoretical discoveries in the quantum interactions of free electrons with light. These fundamental interactions are fully described by a quantum electron wavefunction interacting with a classical electromagnetic field. PINEM-type interactions have demonstrated laser-driven free-electron quantum walk and Rabi oscillations⁴, particle-wave duality with single electrons⁵, laser-controlled electron angular momentum⁶ and photonic cavity lifetime measurement^{7,8}. In such experiments, the electron interacts with the near field of a thin sample and probes its properties. Importantly, the fundamental interaction in all these experiments has remained weak due to the localized nature of the near field, which cannot achieve full energy-momentum matching between electrons and light^{3,9}.

Unlike these quantum localized interactions, extended interactions can become stronger by orders of magnitude when satisfying energy-momentum matching over a long interaction distance and a prolonged interaction duration. This energy-momentum phase-matching condition is famously found in the Cherenkov effect¹⁰, the Smith-Purcell effect¹¹, their inverse effects¹²⁻¹⁸ and a wide range of electron-light interactions that satisfy similar phase-matching conditions¹⁹⁻²². Such classical phase-matching interactions in electrodynamics have been exploited for numerous applications²³ in particle identification²⁴⁻²⁶, medical imaging²⁷, quantum cascade lasers²⁸, optical frequency combs²⁹, laser-driven particles³⁰⁻³² and other areas of nonlinear optics³³ and nanophotonics³⁴⁻³⁷. Yet, to this day, all these free-electron phase-matched experiments have been perfectly accounted for by classical electrodynamics. Fundamentally, all these effects involve the same energy-momentum matching (phase-matching) of a classical particle that interacts

resonantly with a propagating wave over an extended distance of multiple wavelengths, through which the particle exchanges energy with the wave. In a similar way, all demonstrations of analogous effects in a wide range of fields—such as water waves, acoustics, plasmonics and even phononics³⁸—were also explained entirely by classical physics.

A quantum description of phase-matched electron-light interactions resulted in several theoretical predictions of quantum effects. Conceptually, quantum electrodynamics (QED) predicts three different types of quantum effect that can occur in phase-matched electron-light interactions. The first type of effect arises due to quantization of the electromagnetic field; this was first analysed in 1940 by Ginzburg and Sokolov in the context of the Cherenkov effect^{39,40} and was predicted to cause recoil corrections due to photon emission^{41,42}. The second type of quantum effect involves higher-order processes in QED⁴³. The third, which is the most relevant to this work, depends on the quantum-wave nature of the electron. Such quantum corrections can arise from transverse features of the electron wavefunction, such as its orbital angular momentum (OAM)⁴¹, or from longitudinal features of the electron wavefunction, such as its temporal duration^{44,45}. The PINEM interactions can be seen as an occurrence of the quantum effect of the third type, arising from the quantum-wave nature of the electron, yet with localized near fields. So far, none of the three types of quantum effect have been observed with an extended field. It is exactly these types of extended field interaction that are central in laser-driven particle acceleration and in all phase-matched interactions.

In this Article, we report the observation of such a quantum effect: a quantum electron wavefunction interacting with an extended field while satisfying phase-matching conditions (our results first appeared on arXiv on September 2019; ref. ⁴⁶). We demonstrate a resonant exchange of hundreds of photon quanta with a single electron by precisely matching the phase velocity of the light wave and the group velocity of the electron wavefunction along the electron

¹Department of Electrical Engineering, Russell Berrie Nanotechnology Institute and Solid-State Institute, Technion, Israel Institute of Technology, Haifa, Israel. ²These authors contributed equally: Raphael Dahan, Saar Nehemia. ✉e-mail: kaminer@technion.ac.il

trajectory. Our experiment achieves this phase-matched interaction by illuminating the electron at the Cherenkov angle. Under this Cherenkov-type phase-matching condition, parts of the electron wavefunction strongly gain energy, while other parts strongly lose energy simultaneously (Fig. 1). In other words, the same electron simultaneously absorbs and emits hundreds of photons in our experiment. The coherent resonant interaction remains phase-matched over hundreds of micrometres, resulting in a modulated electron wavefunction that forms a quantized plateau extending over hundreds of electron volts. We find that conventional PINEM theory is not sufficient to explain these findings, so we develop a theory that extends beyond the conventional theory and provides a general formalism for all phase-matched electron–light interactions. Revealing quantum features in such interactions shows prospects for the design of highly controllable light sources^{31,47,48}, spectroscopy methods⁴⁹ and more efficient accelerators and detectors^{50–52}.

We compared our measurements with classical theory (Fig. 1b–d), which forms a bridge between PINEM-type experiments and dielectric-laser accelerators (DLAs). DLA experiments also use phase-matched electron–laser interactions; however, a classical theory has accurately described all DLA experiments so far^{30,53,54}. Surprisingly, differences in the classical versus quantum predictions appear most strongly at maximal energy gain and loss (Supplementary Fig. 3). In addition, the energy resolution and electron coherence in our experiments uncover that each electron accelerated by a DLA can potentially become a quantized energy comb. This comparison constitutes an intriguing connection between DLAs and PINEM experiments: they can be seen as two sides—quantum and classical—of the same family of phase-matched electron–laser experiments.

Experimental set-up

To achieve a strong interaction in our experiment, we satisfy the phase-matching condition by reducing the phase velocity of light using a dielectric medium—a glass prism (Fig. 2). The light is coupled into the prism to precisely match the Cherenkov angle θ and undergoes total internal reflection inside the prism. As a result, an evanescent tail extends outside the medium into vacuum, where it interacts with the electron that grazes the prism's interface along several hundred micrometres (Figs. 1a and 2). This grazing-angle interaction is sometimes called the Cherenkov–Landau effect⁵⁵, and was studied in many previous papers using electrons moving in vacuum near a planar interface^{13,18}. In all previous works, such interactions and all interactions that satisfied phase-matching conditions were always described using classical electrodynamics. For example, a prism set-up was used recently³⁰ to achieve the phase-matching condition in classical electrodynamics using a scanning electron microscope. By contrast, our work demonstrates a quantum interaction satisfying phase-matching using a coherent free-electron wavefunction and measuring it with an energy resolution better than the energy of a single photon, thereby revealing the quantum features of the interaction. Such an interaction results in an extraordinarily strong quantized modulation of the electron energy spectrum.

The experimental set-up that we use to demonstrate the strong quantized interaction is an ultrafast transmission electron microscope (UTEM). To achieve the strong phase-matched interaction, besides synchronizing the velocities, the focused electron probe needs to remain in the region of the evanescent field (\lesssim one wavelength from the surface⁵⁶) over a long distance, that is, achieve the grazing-angle interaction (Fig. 2). In our case, this challenge requires aligning the surface with respect to the electron beam, to be precisely parallel to it with error less than $\sim \lambda/2 = 350$ nm for an entire prism side length of 500 μ m. Otherwise, part of the electron beam will either be blocked by the prism or the electron will be too far away to interact with the evanescent field. The electron beam is

also focused to a submicrometre probe to maximize the interaction; however, this comes at the price of a high divergence angle. Despite these complications, we achieved this grazing-angle condition by a technique we developed and applied in the UTEM (Methods), which maximizes the electron–laser interaction to a greater strength than previously achieved in the literature. (The effective interaction length is three orders of magnitude larger than that achieved in previous works owing to our proprietary grazing-angle interaction set-up. Our grazing-angle interaction differs from regular electron microscope experiments in which thin samples are used (tens to a few hundred nanometres).) To the best of our knowledge, the realization of such grazing-angle interaction conditions has not been accomplished previously in a transmission electron microscope (TEM).

The UTEM set-up was previously used to study quantized interactions of free electrons with a laser^{1,4,9,57–60}. All previous UTEM experiments involved a localized interaction^{1,4,57,59}, for example, near fields (as in the PINEM acronym), propagating transverse to the electron velocity^{5,6,60} or spatially limited in other ways⁹. As long as the interaction remains localized, it can be described with conventional PINEM^{2–4,9}. By contrast, our study demonstrates an extended interaction, in both space and time, with propagating electromagnetic waves that accompany the electron motion, which requires a more advanced theory than conventional PINEM.

Extending the theory of PINEM

In conventional PINEM^{2,4,9}, the interaction is quantified by a single dimensionless coupling constant g , which describes the normalized interaction strength. This coupling constant is derived by integration of the (classical) electric field along the electron trajectory $r(t) = (x, y, v_e t)$:

$$g(x, y) = \frac{q_e}{\hbar\omega} \int_{-\infty}^{\infty} \tilde{E}_z(x, y, z) e^{-i\omega z/v_e} dz \quad (1)$$

where \tilde{E}_z is defined by $E_z(t) = \tilde{E}_z e^{-i\omega t}$ (the electric-field z component without its carrier frequency), q_e is the electron charge, ω is the laser frequency and v_e is the electron velocity. This g parameter can be measured with¹ or without⁴ averaging over the electron and laser pulses^{3,9}. Either way, in all PINEM papers so far, the same g parameter was the fundamental measure of the interaction strength. However, this fundamental parameter cannot describe our experiment because of the prolonged duration and extended length of the interaction; these conditions in our grazing-angle experiments force us to extend PINEM theory.

To capture a general extended time-dependent interaction, we can define a generalized g parameter that is now also a function of a time variable T that parameterizes the electron trajectory:

$$g(x, y, T) = \frac{q_e}{\hbar\omega} \int_{-\infty}^{\infty} \tilde{E}_z(x, y, z, T + z/v_e) e^{-i\omega z/v_e} dz \quad (2)$$

Comparing to equation (1), \tilde{E}_z is now time-dependent. This expression contains the parameterization of the electron trajectory (the z parameter), not only in the spatial coordinate of $\tilde{E}_z(x, y, z, z/v_e + T)$, but also in its temporal coordinate, which represents the temporal dynamics of the laser field. This time variable in $g(x, y, T)$ encodes the dependence of the interaction strength on the dynamics of the electromagnetic field that accompanies the electron along its extended trajectory. For more details see Supplementary Note 1 and for an illustration of the dynamics see the Supplementary Video.

With this generalized g parameter, the electron wavefunction (under a paraxial approximation as in conventional PINEM^{2,3} and in our Supplementary Note 1) can be expressed as

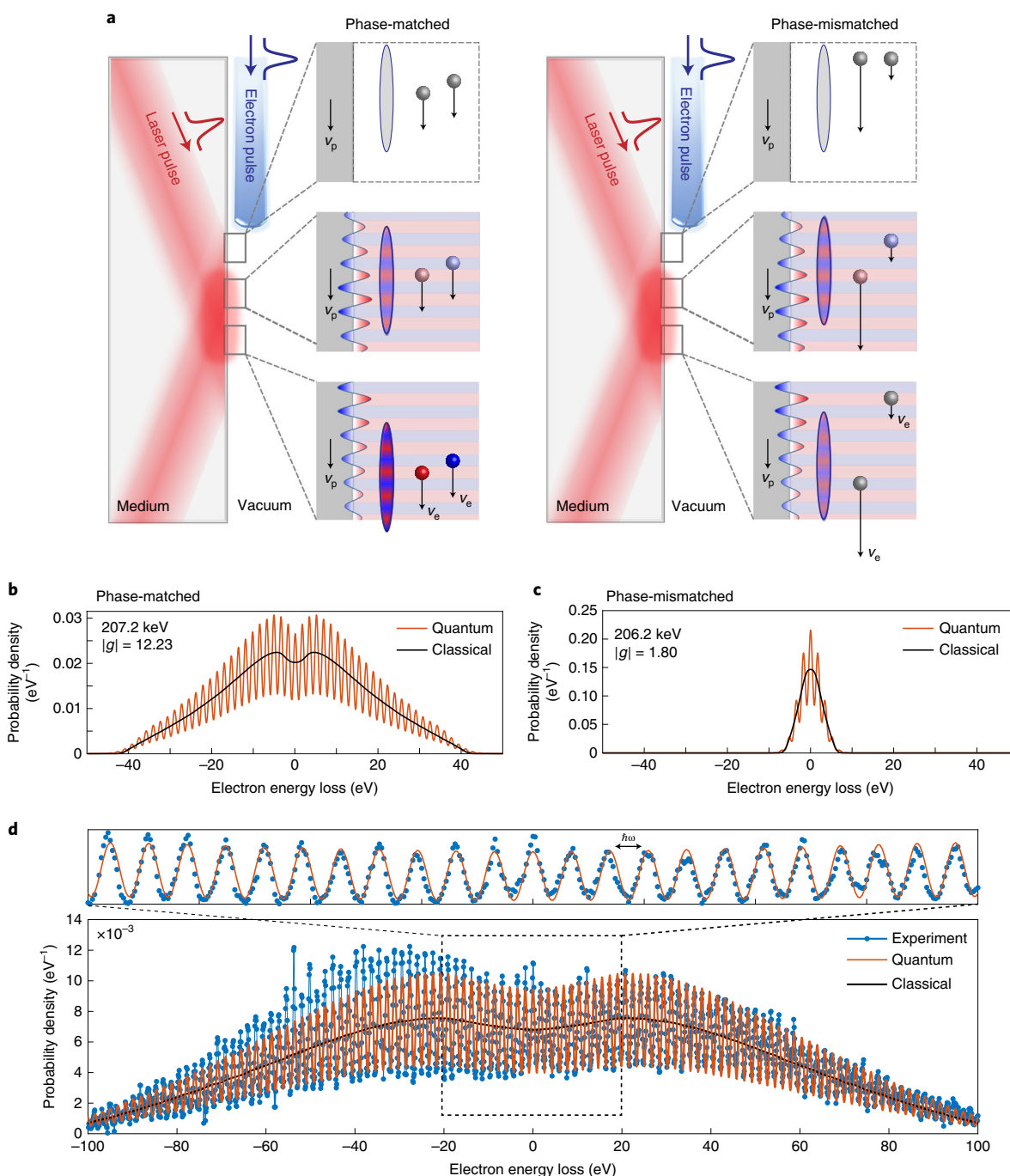


Fig. 1 | Quantum versus classical phase-matching of an electron and light. A demonstration of a quantum Cherenkov effect; our experimental results show the strong quantum interaction of the electron wavefunction with the phase-matched field achieved by fine-tuning of the electron velocity v_e to match the phase velocity of light v_p . **a**, Comparison of the phase-matched interaction (left) and an interaction that is not phase-matched (right), for both the classical and quantum interpretations. The electron interacts with an evanescent field generated by a laser that is totally internally reflected from a planar interface. In the classical interpretation, a point electron is phase-matched with the alternating amplitude of the light field (red/blue) and results in accumulated acceleration/deceleration. In the quantum interpretation, an electron wavefunction (shown in its spatial representation) is phase-matched with a propagating light field over multiple optical wavelengths/cycles simultaneously, leading to a phase modulation of the electron wavefunction (alternating red–blue colouring) that directly translates to the electron energy change. When the phase-matching condition is satisfied, each point in the electron wavefunction interacts with a different part of the field, yet always in a resonant manner. Note that the phase-matching condition is the same for classical and quantum theory. **b, c**, Comparison of the resulting electron energy spectra when phase-matched (**b**) and phase-mismatched (**c**). The classical spectrum approximates the average of the quantum spectrum, except for the far edges of the spectrum (Supplementary Fig. 3). **d**, Example of our measured (blue) and theoretical (orange) electron energy spectrum after a phase-matched interaction. The spectrum shows an energy gain/loss of 100 eV discretized by quanta of photon energy ($\hbar\omega \approx 1.7$ eV). Figure 5 (later) shows the results of larger gain and loss. The quantum (orange) and classical (black) calculated spectra are also provided for comparison, showing a good fit to the acquired spectrum; for details see Supplementary Notes 1 and 3, respectively. Top: zoom in on the range -15 to 15 eV to highlight individual peaks.

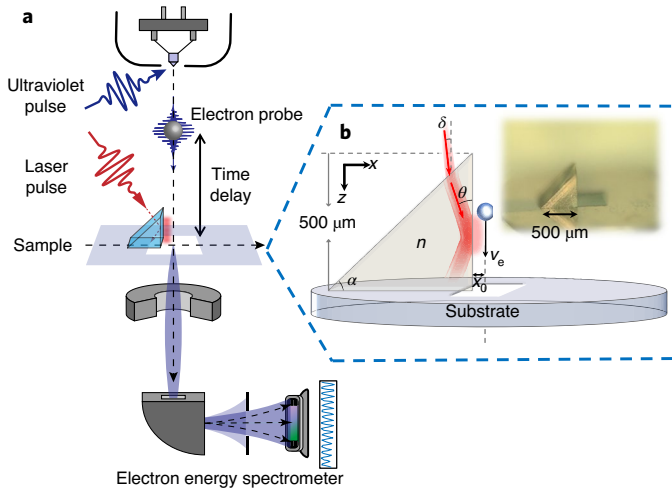


Fig. 2 | Experimental set-up. **a**, Illustration of the UTEM set-up, showing the grazing-angle interaction with a prism. The electron pulse is generated by photoexcitation of electrons with an ultraviolet pulse. The electrons graze the surface of a prism and interact with an evanescent field generated by another laser pulse that enters the prism and undergoes total internal reflection from the same surface. The electrons are measured with an electron energy spectrometer. **b**, Zoom in on the interaction area along the planar interface of a prism ($\alpha = 45^\circ$). The laser illuminates the electron at the Cherenkov angle $\theta = 19.8^\circ$, satisfying $n \cos \theta = c/v_e$, with n being the index of refraction of the prism and v_e the electron velocity. Inset: image of the prism positioned on the edge of a hole through which the electrons pass (parameters are defined in the Methods).

$$\begin{aligned} \phi(x, y, T) &= \phi_0(x, y, T) e^{-2i\text{Im}\{g(x, y, T)e^{-i\omega T}\}} \\ &= \phi_0(x, y, T) \sum_{\ell=-\infty}^{\infty} J_{\ell}(2|g(x, y, T)|) e^{i\ell \arg\{-g(x, y, T)\}} e^{-i\ell\omega T} \end{aligned} \quad (3)$$

where ϕ_0 is the coherent envelope of the electron wavefunction before the interaction. Note that, unlike conventional PINEM theory, the analytical expansion in equation (3) is not a Fourier series, because the coefficients depend on T , and thus the Bessel functions $J_{\ell}(2|g(x, y, T)|)$ cannot represent amplitudes of the electron quantum state on the energy ladder. To extract the electron energy spectrum, we can convert equation (3) into a Fourier transform, showing how each previously discrete PINEM energy ladder is coherently broadened into a continuous energy distribution (by the laser linewidth in g). For large values of g , this phenomenon changes the electron energy spectrum, deviating from conventional PINEM theory.

Using the time-dependent coupling constant $g(x, y, T)$, we derive the energy probability density of the electron after the interaction $\rho(x, y, U, \Delta t)$ at different time delays Δt and energies U . We do so by convolving, in both energy and time, the probability density that resulted from a coherent interaction with the probability density of the incoming electron $\rho_0(x, y, U, T)$:

$$\begin{aligned} \rho(x, y, U, \Delta t) &= \\ \int dU dT \rho_0(x, y, U, T) &\sum_{\ell=-\infty}^{\infty} J_{\ell}^2(2|g(x, y, \Delta t - T)|) \delta(U - U - \ell\hbar\omega) \end{aligned} \quad (4)$$

$\rho_0(x, y, U, T)$ contains the experimental values of the incoherent energy width (the zero-loss peak), the incoherent pulse duration

of the incoming electron, as well as the spot size and location of the electron probe. We average the probability distribution over x, y by $\rho(U, \Delta t) = \int dx dy \rho(x, y, U, \Delta t)$; for more information see Supplementary Notes 1 and 5c. Note that, in equation (4), we neglect the coherent energy broadenings of the interaction relative to the incoherent energy width of the incoming electron.

Figure 3 presents a map of the electron energy spectrum $\rho(U, \Delta T)$ as a function of delay ΔT between the electron and laser pulses (the time delay scan). By incorporating the spatiotemporal dynamics of the laser field, our extended PINEM theory explains the acquired data better than conventional PINEM theory (compare the panels in Fig. 3). Importantly, our time-dependent coupling constant $g(x, y, T)$ (equation (2)) reduces to the time-independent $g(x, y)$ (equation (1)) of conventional theory^{2-4,9}, when assuming a separable coupling constant $g(x, y, T) = g(x, y) \cdot \text{func}(T)$, with func representing the longitudinal spatiotemporal profile of the laser pulse. However, this assumption is invalid in our experiment and the implications are shown in the comparison in Fig. 3c,d. The most prominent difference is that, while conventional theory predicts energy gain and loss of up to ~ 270 eV, both the extended theory and the experiment show an energy gain and loss up to ~ 500 eV.

Satisfying the phase-matching condition over hundreds of micrometres

In the present set-up, the electron interacts with an evanescent wave that can be expressed as $\tilde{E}_z(x, y, z, t) = \tilde{E}_{\text{envelope}}(x, y, z, t) e^{-k_x x} e^{ik_z z}$ ($k_x > 0, k_z > 0$), where $(k_x = ik_x, k_y = 0, k_z)$ is the wavevector of the evanescent field and $\tilde{E}_{\text{envelope}}(x, y, z, t)$ is the envelope, for example, arising from the Gaussian pulse (Supplementary Note 2). Once we substitute the field into equation (2), the z coefficient in the exponent becomes $k_z - \omega/v_e$, which expresses the phase-mismatch between the electron and the field.

The key to realizing the resonant strong interaction is to maintain the phase-matching condition $v_e = \omega/k_z$ for a long interaction along the planar interface. Satisfying this phase-matching condition is equivalent to a condition on the angle of the incident laser to equal the famous Cherenkov angle, that is, $\cos \theta = c/(v_e n)$, with n being the index of refraction (Fig. 2b and Supplementary Note 4). When the condition is satisfied, a long interaction length results in a coupling constant that grows linearly with the system macroscopic size. (With the phase-matching condition satisfied, the integrand in equation (2) is no longer periodic and instead of canceling out after every period of the field it is accumulated over the periods. Therefore, it seems that g would diverge for an infinite interaction length, but, in practice, it is bounded by the finite length of the interaction.) This linear scaling is different from all the previous PINEM experiments and it is the key for the strong interaction we observe. In all these previous experiments, only a single Fourier component of the near field contributed to the coupling constant; the rest of the field did not participate in the interaction. By contrast, in our experiment, the entire field constitutes a single Fourier component and thus contributes to the strong interaction. This difference in scaling is exactly analogous to the situation in many nonlinear optical processes such as second-harmonic generation. There, without satisfying the phase-matching condition, the efficiency is extremely weak; however, once the phase-matching condition is satisfied the efficiency grows linearly with system size.

Quantitatively, we can define an effective interaction length L_{eff} such that $|g| = \frac{q_e E_0 z L_{\text{eff}}}{\hbar \omega}$. In all previous experiments the interaction was localized (for example, refs. 1,4,9,60) and the effective length of interaction was roughly $L_{\text{eff}} \lesssim \lambda$ (several hundred nanometres). However, our grazing-angle conditions enable us to increase this to $L_{\text{eff}} \gg \lambda$ (several hundred micrometres) by exploiting the phase-matching in an extended interaction using our grazing-angle set-up. As a result, we achieved a large coupling constant g (Fig. 5), more than an order of magnitude larger than in previous PINEM experiments.

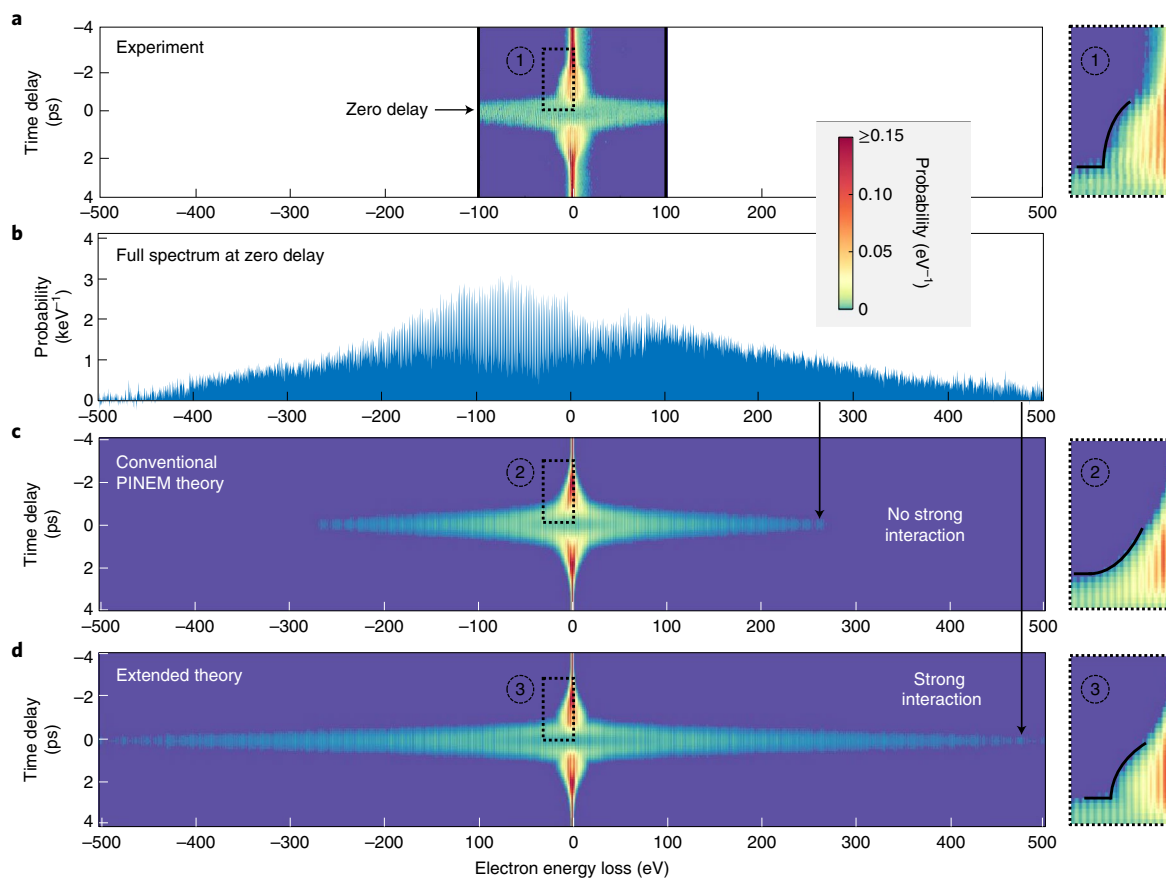


Fig. 3 | Comparison of the experimental data with both conventional PINEM theory and our extended theory. **a**, Experimental time delay scan of the electron energy spectrum, varying the delay between the laser and electron pulses (energy range of -100 to 100 eV). **b**, Full electron energy spectrum at zero delay (energy range of -500 to 500 eV). **c**, Simulated time delay scan produced using conventional PINEM theory. This theory neglects the temporal dynamics of the laser pulse during its extended interaction with the electron. The simulated time scan is far from the experimental results (**a**, **b**), as it predicts a maximum interaction strength of less than 300 eV. **d**, Simulated time delay scan produced using our extended theory, which accounts for the temporal evolution of the laser pulse during its extended interaction with the electron. The electron and laser pulses overlap for a prolonged duration and distance, resulting in a much broader electron energy spectrum that shows good agreement with the experimental data. The insets to the right of **a**, **c** and **d** show zooms of the top left corner of each scan (marked by dashed rectangles). The two theories produce opposite curvatures, and only the extended theory matches the experiment (solid black curves are marked to guide the eye). The energy probability distribution $\rho_0(x, y, U, t)$ of the initial electron has a Gaussian profile in time (~ 400 -fs full-width at half-maximum, FWHM) and energy (~ 1.1 -eV FWHM).

Figure 4 analyses the effect of different parameters on the phase-matching and emphasizes the sensitivity of the interaction strength to the electron energy. The acceleration voltage controls the electron kinetic energy ($E_e = 207.2$ keV) and determines its velocity ($v_e = 0.7027c$). Because of material dispersion, the refractive index of the prism changes with the laser wavelength; for example, $n = 1.512$ at $\lambda = 730$ nm. The strongest interaction at each wavelength in Fig. 4a follows a curve that satisfies the resonant phase-matching condition: a small change of only 2 keV ($<1\%$) in the electron energy can result in g changing by an order of magnitude. The level of sensitivity is proportional to the interaction length. The electron energy spectra in Fig. 4c–e highlight the importance of precise phase-matching for the interaction strength: roughly, the maximum number of photons exchanged is $2|g|$ and the energy spread (the edge of each spectrum) is $2\hbar\omega|g|$. The theoretical analysis is provided in Supplementary Note 1.

An optimal interaction has to balance important tradeoffs: the interaction is indeed stronger for longer wavelengths (Fig. 4a), but the quantum features are harder to measure because the distance between adjacent peaks shrinks (insets, Fig. 4c–e). Another trade-off is that a longer medium interface increases g but also requires that the electron stays farther away from the interface because of

its unavoidable spread angle (Fig. 4b), which creates an exponential decrease in the interaction strength (dashed lines, Fig. 4b). (The effective interaction length is limited in practice by the length of the medium, the transverse spatial extent of the incident laser pulse (initial spot size) projected on the prism's surface, and the temporal duration of the laser pulse; Supplementary Notes 2 and 4.)

Figure 5 shows measurements of strong interactions with the large g values that resulted from the Cherenkov phase-matched interaction. In the blue curve in Fig. 5a we achieved $|g| \approx 150$, which matches the maximum energy gain/loss of 510 eV (also see the zoomed panels in Fig. 5b and the comparison with theory in Fig. 5c). By using a shorter duration and a more intense laser pulse, we achieved $|g| > 250$, which matches a maximum energy gain/loss of <850 eV (that is, $>1,700$ eV bandwidth, pink energy spectra in Fig. 5a). However, this interaction involves only part of the electron distribution, leaving a large near-zero peak in the electron energy spectrum. Regardless, the interaction results in a free-electron comb where the electron exchanges hundreds of photons with the field, becoming a coherent superposition of energy peaks in the form of a quantized plateau (Fig. 5b).

Notably, Fig. 5 shows that the quantization of the electron energy spectrum in the form of a comb can spread over more

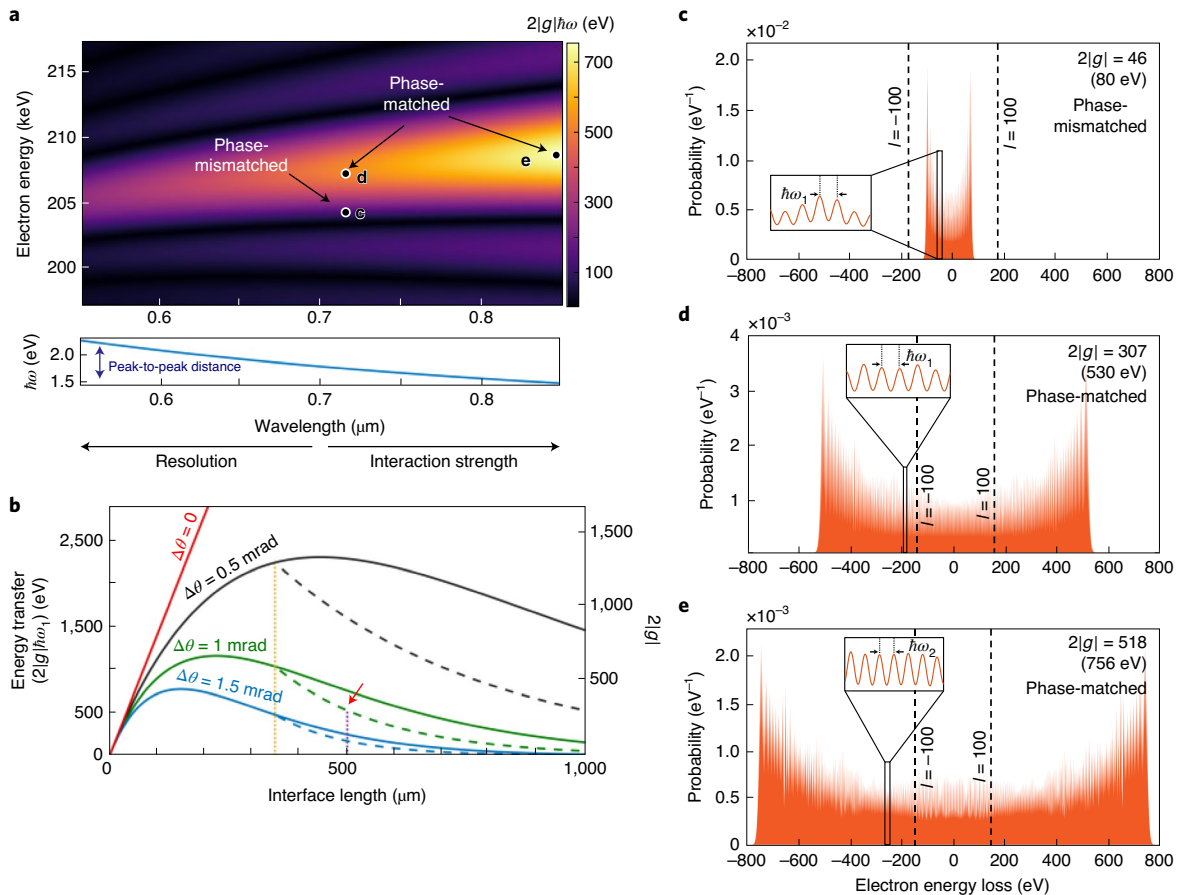


Fig. 4 | Conditions for phase-matching and theoretical analysis. **a**, The interaction strength quantified by the energy spread $2|g|\hbar\omega$ as a function of the electron kinetic energy and the wavelength of the laser, showing the curve of perfect phase-matching. Bottom: reminder of photon energy versus wavelength to emphasize that the distance between peaks in the spectra changes with the wavelength. As we increase the wavelength, we obtain a stronger interaction but gradually lose the ability to resolve individual peaks. **b**, The interaction strength as a function of the prism length for different divergence angles of the electron beam ($\Delta\theta = 0$ is a perfectly collimated beam). By fitting our data, we estimate a beam divergence of $\Delta\theta \approx 1 \text{ mrad} = 0.057^\circ$. This parameter also includes a deviation from a perfect straight trajectory, because the beam follows a helical trajectory created by the magnetic field of the objective lens. This divergence keeps the electron beam farther away from the prism for larger interface lengths, which explains the eventual decay of all curves except for the perfectly collimated beam. A threshold length is set by the laser spot size projected on the interface ($\approx 350 \mu\text{m}$, yellow dotted line), above which an increase in the length of the interface results only in a decay in g (dashed curves). Red arrow: the point at which we work in our experiment. **c–e**, Examples of electron energy spectra calculated with different coupling constants showing weak (**c**, $E_e = 204.5 \text{ eV}$, $\lambda_1 = 730 \text{ nm}$ (1.7 eV)), intermediate (**d**, $E_e = 207.2 \text{ eV}$, $\lambda_1 = 730 \text{ nm}$ (1.7 eV)) and strong (**e**, $E_e = 208.5 \text{ eV}$, $\lambda_2 = 850 \text{ nm}$ (1.46 eV)) interaction strengths, respectively. The calculations for this figure use our experimental parameters unless stated otherwise (see Methods for more information).

than a thousand electron volts. An electron energy comb has been observed previously only in pulsed photoexcitation of bound electrons, as in the phenomenon of above-threshold ionization⁶¹ (ATI). Such spectral features in electrons are the reason for the production of a similar comb of high laser harmonics, which opened the field of attosecond science⁶². All these rely on initially bound electrons that absorb multiple photons, but never on free electrons. Free electrons have remarkably different physical phenomena and applications compared to bound electrons. For example, unlike bound electrons, free electrons can have relativistic velocities and therefore induce relativistic effects, such as the quantum physics of DLA and of Cherenkov-type interactions that we observed in this work. More generally, the resonant phase-matched interaction we explored opens the way to extremely nonlinear quantum optical phenomena based on free electrons.

Discussion

Our measurement of the electron energy spectrum reveals the quantum nature of stimulated emission and the absorption

processes of phase-matched free electrons. Specifically, we find quantum features that arise from the electron having a longitudinal wavefunction instead of just being a point particle. (It has been shown (for example, in ref.⁵⁰) that, by applying a PINEM-like formalism on an electron wavefunction that is shorter than the optical cycle/wavelength, the electron energy spectrum becomes similar to the classical one.) These results conform to theoretical predictions about the dependence of stimulated emission on the quantum wavefunction of the emitting electron^{44,45}. Nevertheless, the prospects and mere possibility of spontaneous emission depending on the wavefunction⁶³ still require further research (because it has not been observed yet): one experiment on free-electron spontaneous radiation emission showed no wavefunction dependence⁶⁴, in contrast to another experiment on spontaneous near-field excitations (rather than radiation emission) that did show such dependence⁶⁵. These experiments motivate an intriguing future work that can be done in a UTEM: the measurement of spontaneous Cherenkov radiation emission that should accompany the measured (stimulated) inverse-Cherenkov effect. Interestingly, because the electron

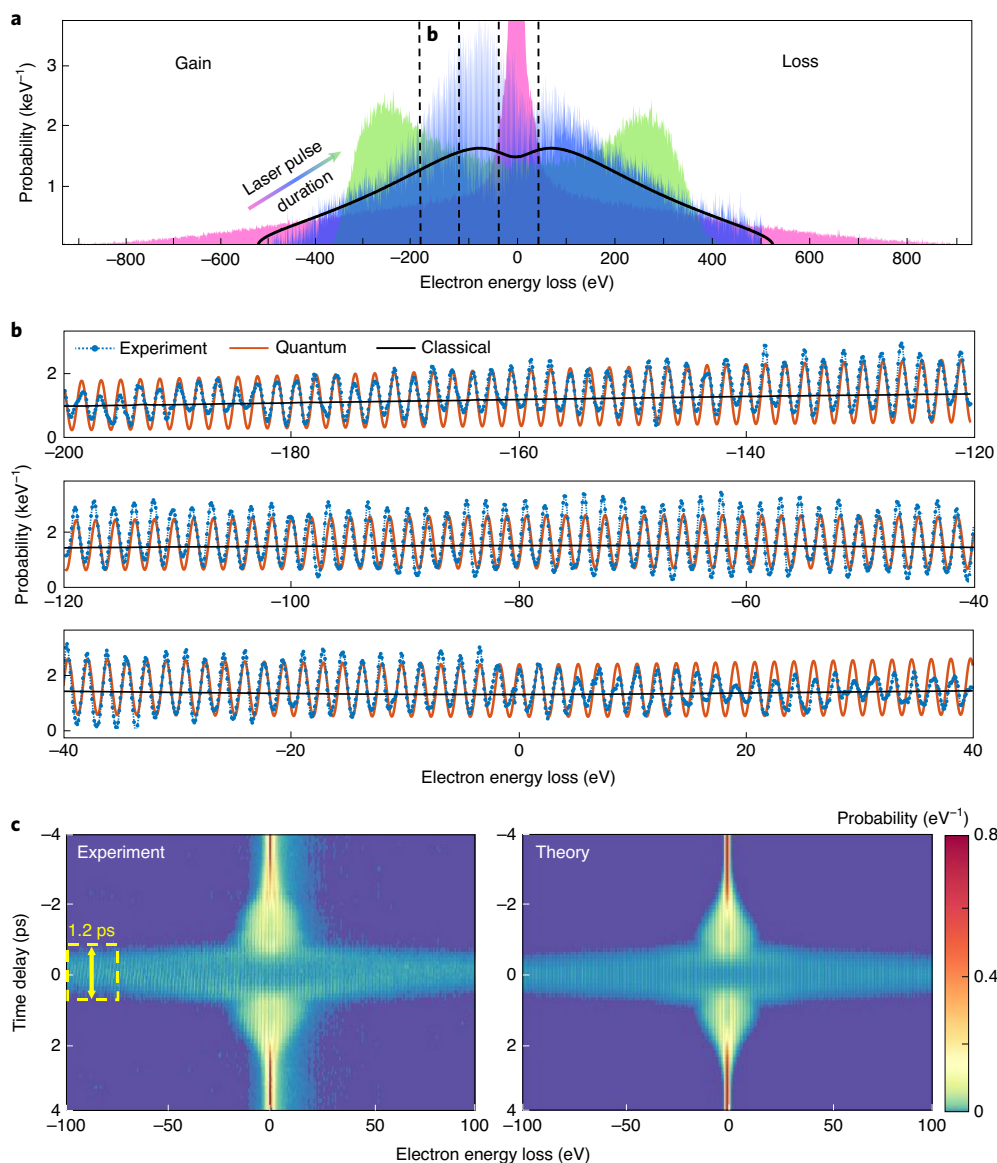


Fig. 5 | Experimental results showing the coherent electron energy comb forming a plateau or energy peaks. The strong interaction is presented as a function of the time delay between the electron and the laser pulses. **a**, Acquired electron energy spectra for different laser pulse durations (pink 280 fs, blue 600 fs, green 1,300 fs), while the electron pulse duration is kept unchanged. As we increase the laser pulse duration, the entire electron distribution feels the same laser amplitude, which creates a double-peaked structure in the electron energy spectrum (green). As we decrease the laser pulse duration and thereby increase its peak intensity, the maximal energy exchange increases to >850 eV, that is, a bandwidth of $>1,700$ eV (pink), and yet, only part of the electron distribution feels the maximal laser field. **b**, Magnification of the blue spectrum in **a**, with comparison to quantum theory and classical theory (described in Supplementary Notes 1 and 2). Note that the quantum theory conforms to the classical case in the limit where the electron wavefunction is smaller than the optical cycle/wavelength⁵²; however, this limit does not fit our experimental data. We were able to resolve individual quantized peaks over a range of hundreds of eV by capturing slices in high resolution and shifting the range of the spectrometer to collect the entire spectrum slice by slice. **c**, Experimental and theoretical time delay scans, varying the delay between the laser and electron pulses. We obtain a good match between theory and experiment by modelling the laser's temporal pulse profile to incorporate changes by our optical parametric amplifier and by considering the spatiotemporal dependence of both the electron and laser pulses in extended PINEM theory. (The optical parametric amplifier changes the laser's temporal pulse shape and adds temporal side lobes on the two sides of the center Gaussian-like pulse. These side lobes explain the features seen in the time scan at time delays before and after the main interaction.) We find a prolonged interaction duration of 1.2 ps due to the dynamics of the laser pulse envelope that partially accompanies the electron (marked in yellow on the left side of **c**). This amount is defined as the median duration when the signal drops to 10% of its maximum value in all energy cuts between -100 eV and -80 eV. All the other results in this work are presented at the point of maximal interaction (time zero).

has been modulated into a comb of energy peaks, the subsequent Cherenkov emission may also be composed of multiple radiation orders at different angles and frequencies.

We successfully modelled the experiment by describing the phase-matching condition between the field of the incident laser

and the electron wavefunction. Interestingly, it is also possible to describe such interactions as arising between the field of the incident laser and the field accompanying the electron. Both descriptions of phase-matching are equivalent, as the velocity of the electron is equivalent to the velocity of the wave accompanying it.

The description based on the accompanying field was found to be useful in describing a range of emission processes in electron beam physics (for example, transition radiation and Cherenkov radiation)—by calculating the scattering of the field accompanying the electron by the optical medium⁶⁶. Although this equivalence of the two phase-matching approaches is well understood in the classical case, it was not previously shown rigorously to be equivalent in the quantum case. The challenge is that one should capture the field accompanying the quantum electron wavefunction and match the phase velocity of this (now quantum) accompanying field with the phase velocity of the external driving field.

Our extended phase-matching can enhance a wide range of applications of coherent free-electron–light interactions. For example, the creation of electron attosecond pulses^{58,67–69} can now be enhanced by phase-matching in grazing-angle conditions. The result would be more than a thousand individual pulses, all part of the same single electron. Because coupling constants of $g \approx 5$ can lead to electron pulse durations shorter than 100 as, a coupling constant of $g \approx 500$, not far from what we have demonstrated here, will create electron combs with subattosecond timescales—a long-held goal⁹ for exploring zeptosecond science. Future experiments with better alignment, longer interaction and higher laser intensities would inevitably result in even narrower electron pulses and a wider plateau of quantized energy peaks.

Our extended PINEM theory shows a good match between simulations and experiments for the electron energy spectrum (Fig. 5c). Yet, in some cases, as in Fig. 1d, we notice an asymmetry between the gain and loss sides in our measured spectrum, which does not appear in the theory. This asymmetry may potentially be explained by several different mechanisms: the chirp of the laser pulse creating an asymmetric phase shift that is accumulated along the extended interaction; electron dispersion that detunes parts of the wavefunction from perfect phase-matching along the extended propagation and breaks the approximations used in both conventional PINEM theory and our extended theory; energy loss mechanisms such as bulk plasmon emission and core losses; harmonics of the field created by some nonlinear effects in the prisms; spontaneous radiation by the interacting electron. Our model can be generalized to capture these effects (for a further discussion see Supplementary Notes).

The phase-matching condition we obtain from the Cherenkov condition is analogous to the phase-matching utilized in DLAs^{53,54}. In DLAs, a tailor-designed laser-driven nanophotonic structure can accelerate particles with gradients of up to a few keV per micrometre when driven by a high enough intensity (orders of magnitude above the intensities we used in our proof-of-concept experiment). In our case, it is the evanescent mode propagating along the surface of the prism that acts as the effective means of acceleration instead of a tailored-design nanophotonic DLA structure. This analogy shows that UTEM systems can complement the existing experimental set-ups used for testing DLA devices (our system operates at 40–200 keV), providing a way to study the quantum nature of the DLA.

Intriguingly, our work shows that the quantum-wave nature of the electron provides an additional degree of control to the acceleration process in DLAs, thereby opening up intriguing avenues of research on these systems. The comparison of quantum theory with the conventional classical⁵⁰ one shows fine details in the energy spectrum (individual energy peaks). More importantly, the quantum theory also provides a more accurate prediction of the regimes of highest energy gain and energy loss (Supplementary Note 3 and Supplementary Fig. 3). DLA experiments have not been able to observe their quantum nature so far due to the limited energy resolution. Therefore, it is not known whether such DLA systems also have quantized electron spectral features or whether limited coherence of the accelerated electron eliminates such an effect. Consequently, it will be interesting to explore further implications

of this analogy between DLA and PINEM and explore the conditions in which the quantum nature of the electron may influence the design of future DLAs.

Looking at the bigger picture, analogous phase-matching conditions appear in other free-electron interactions, such as the (inverse-) Smith–Purcell effect and various undulator concepts^{16,19–22}. In all experimental work on these effects, the electron has always been considered to be a classical point charge. We now show a regime where these kinds of effect are essentially quantum and require the electron to be a wavefunction to correctly explain the experiments. Future experiments analogous to our work here are expected to reveal underlying quantum-wave effects and quantized electron energy exchanges in all these systems.

We envision combining the elongated phase-matched interaction in this Article with an elongated photonic cavity as a route to achieving an efficient single-electron–single-photon interaction^{70,71} and possibly even ultrastrong free-electron–light coupling⁴³. The cavity will channel emitted photons that can then be resonantly reabsorbed by the extended electron, creating a strongly coupled electron–photon hybrid. This hybrid will enable the exploration of previously unknown processes such as free-electron Lamb shifts, extreme mass renormalizations and potentially even cavity-mediated Cooper pairs of free electrons.

Online content

Any methods, additional references, Nature Research reporting summaries, source data, extended data, supplementary information, acknowledgements, peer review information; details of author contributions and competing interests; and statements of data and code availability are available at <https://doi.org/10.1038/s41567-020-01042-w>.

Received: 21 April 2020; Accepted: 14 August 2020;

Published online: 12 October 2020

References

- Barwick, B., Flannigan, D. J. & Zewail, A. H. Photon-induced near-field electron microscopy. *Nature* **462**, 902–906 (2009).
- García de Abajo, F. J., Asenjo-García, A. & Kociak, M. Multiphoton absorption and emission by interaction of swift electrons with evanescent light fields. *Nano Lett.* **10**, 1859–1863 (2010).
- Park, S. T., Lin, M. & Zewail, A. H. Photon-induced near-field electron microscopy (PINEM): theoretical and experimental. *New J. Phys.* **12**, 123028 (2010).
- Feist, A. et al. Quantum coherent optical phase modulation in an ultrafast transmission electron microscope. *Nature* **521**, 200–203 (2015).
- Piazza, L. et al. Simultaneous observation of the quantization and the interference pattern of a plasmonic near-field. *Nat. Commun.* **6**, 6407 (2015).
- Vanacore, G. M. et al. Ultrafast generation and control of an electron vortex beam via chiral plasmonic near fields. *Nat. Mater.* **18**, 573–579 (2019).
- Wang, K. et al. Coherent interaction between free electrons and a photonic cavity. *Nature* **582**, 50–54 (2020).
- Kfir, O. et al. Controlling free electrons with optical whispering-gallery modes. *Nature* **582**, 46–49 (2020).
- Vanacore, G. M. et al. Attosecond coherent control of free-electron wave functions using semi-infinite light fields. *Nat. Commun.* **9**, 2694 (2018).
- Cherenkov, P. A. Visible emission of clean liquids by action of γ radiation. *Dokl. Akad. Nauk SSSR* **2**, 451 (1934).
- Smith, S. J. & Purcell, E. M. Visible light from localized surface charges moving across a grating. *Phys. Rev.* **92**, 1069 (1953).
- Ginzburg, V. L. & Frank, I. M. Radiation of electrons and atoms moving along the axis of a tube in a dense medium. in. *Dokl. Akad. Nauk SSSR* **56**, 699–702 (1947).
- Danos, M., Geschwind, S., Lashinsky, H. & Van Trier, A. Čerenkov effect at microwave frequencies. *Phys. Rev.* **92**, 828–829 (1953).
- Fontana, J. R. & Pantell, R. H. A high-energy, laser accelerator for electrons using the inverse Cherenkov effect. *J. Appl. Phys.* **54**, 4285–4288 (1983).
- Piestrup, M. A. An analysis of oblique angle stimulated Cherenkov radiation with some experimental results. *IEEE J. Quantum Electron.* **19**, 1827–1834 (1983).
- Mizuno, K., Pae, J., Nozokido, T. & Furuya, K. Experimental evidence of the inverse Smith–Purcell effect. *Nature* **328**, 45–47 (1987).

17. Kimura, W. D. et al. Laser acceleration of relativistic electrons using the inverse Cherenkov effect. *Phys. Rev. Lett.* **74**, 546–549 (1995).
18. García De Abajo, F. J., Rivacoba, A., Zabala, N. & Yamamoto, N. Boundary effects in Cherenkov radiation. *Phys. Rev. B* **69**, 155420 (2004).
19. Schächter, L. *Beam-Wave Interaction in Periodic and Quasi-Periodic Structures* (Springer, 1997).
20. Friedman, A., Gover, A., Kurizki, G., Ruschin, S. & Yariv, A. Spontaneous and stimulated emission from quasifree electrons. *Rev. Mod. Phys.* **60**, 471–535 (1988).
21. Mizrahi, A. & Schächter, L. Optical Bragg accelerators. *Phys. Rev. E* **70**, 016505 (2004).
22. Kamner, I. et al. Spectrally and spatially resolved Smith–Purcell radiation in plasmonic crystals with short-range disorder. *Phys. Rev. X* **7**, 011003 (2017).
23. Shaffer, T. M., Pratt, E. C. & Grimm, J. Utilizing the power of Cerenkov light with nanotechnology. *Nat. Nanotechnol.* **12**, 106–117 (2017).
24. Galbraith, W. & Jelley, J. V. Light pulses from the night sky associated with cosmic rays. *Nature* **171**, 349–350 (1953).
25. Ypsilantis, T. & Seguinot, J. Theory of ring imaging Cherenkov counters. *Nucl. Inst. Methods Phys. Res. A* **343**, 30–51 (1994).
26. Lin, X. et al. Controlling Cherenkov angles with resonance transition radiation. *Nat. Phys.* **14**, 816–821 (2018).
27. Ruggiero, A., Holland, J. P., Lewis, J. S. & Grimm, J. Cerenkov luminescence imaging of medical isotopes. *J. Nucl. Med.* **51**, 1123–1130 (2010).
28. Vijayraghavan, K. et al. Broadly tunable terahertz generation in mid-infrared quantum cascade lasers. *Nat. Commun.* **4**, 2021 (2013).
29. Brasch, V. et al. Photonic chip-based optical frequency comb using soliton Cherenkov radiation. *Science* **351**, 357–360 (2016).
30. Kozák, M. et al. Acceleration of sub-relativistic electrons with an evanescent optical wave at a planar interface. *Opt. Express* **25**, 19195–19204 (2017).
31. Gover, A. et al. Superradiant and stimulated-superradiant emission of bunched electron beams. *Rev. Mod. Phys.* **91**, 035003 (2019).
32. Edighoffer, J. A., Kimura, W. D., Pantell, R. H., Piestrup, M. A. & Wang, D. Y. Observation of inverse Cherenkov interaction between free electrons and laser light. *Phys. Rev. A* **23**, 1848–1854 (1981).
33. Zembrod, A., Puell, H. & Giordmaine, J. A. Surface radiation from non-linear optical polarisation. *Opto-Electron.* **1**, 64–66 (1969).
34. Luo, C., Ibanescu, M., Johnson, S. G. & Joannopoulos, J. D. Cerenkov radiation in photonic crystals. *Science* **299**, 368–371 (2003).
35. García de Abajo, F. J. et al. Cherenkov effect as a probe of photonic nanostructures. *Phys. Rev. Lett.* **91**, 143902 (2003).
36. Adamo, G. et al. Light well: a tunable free-electron light source on a chip. *Phys. Rev. Lett.* **103**, 113901 (2009).
37. Genevet, P. et al. Controlled steering of Cherenkov surface plasmon wakes with a one-dimensional metamaterial. *Nat. Nanotechnol.* **10**, 804–809 (2015).
38. Andersen, T. I. et al. Electron–phonon instability in graphene revealed by global and local noise probes. *Science* **364**, 154–157 (2019).
39. Ginzburg, V. L. Quantum theory of radiation of electron uniformly moving in medium. *Zh. Eksp. Teor. Fiz.* **10**, 589–600 (1940).
40. Sokolov, A. Quantum theory of Cherenkov effect. *Dokl. Akad. Nauk SSSR* **28**, 415–417 (1940).
41. Kamner, I. et al. Quantum Čerenkov radiation: spectral cutoffs and the role of spin and orbital angular momentum. *Phys. Rev. X* **6**, 011006 (2016).
42. Tsesses, S., Bartal, G. & Kamner, I. Light generation via quantum interaction of electrons with periodic nanostructures. *Phys. Rev. A* **95**, 013832 (2017).
43. Roques-Carnes, C., Rivera, N., Joannopoulos, J. D., Soljačić, M. & Kamner, I. Nonperturbative quantum electrodynamics in the Cherenkov effect. *Phys. Rev. X* **8**, 041013 (2018).
44. Talebi, N. Schrödinger electrons interacting with optical gratings: quantum mechanical study of the inverse Smith–Purcell effect. *New J. Phys.* **18**, 123006 (2016).
45. Gover, A. & Pan, Y. Dimension-dependent stimulated radiative interaction of a single electron quantum wavepacket. *Phys. Lett. A* **382**, 1550–1555 (2018).
46. Nehemia, S. et al. Observation of the stimulated quantum Cherenkov effect. Preprint at <https://arxiv.org/pdf/1909.00757.pdf> (2019).
47. Talebi, N. Interaction of electron beams with optical nanostructures and metamaterials: from coherent photon sources towards shaping the wave function. *J. Opt.* **19**, 103001 (2017).
48. Rivera, N., Wong, L. J., Joannopoulos, J. D., Soljačić, M. & Kamner, I. Light emission based on nanophotonic vacuum forces. *Nat. Phys.* **15**, 1284–1289 (2019).
49. Polman, A., Kociak, M. & García de Abajo, F. J. Electron-beam spectroscopy for nanophotonics. *Nat. Mater.* **18**, 1158–1171 (2019).
50. Tsarev, M. V. & Baum, P. Characterization of non-relativistic attosecond electron pulses by transition radiation from tilted surfaces. *New J. Phys.* **20**, 033002 (2018).
51. Baum, P. Quantum dynamics of attosecond electron pulse compression. *J. Appl. Phys.* **122**, 223105 (2017).
52. Pan, Y., Zhang, B. & Gover, A. Anomalous photon-induced near-field electron microscopy. *Phys. Rev. Lett.* **122**, 183204 (2019).
53. Peralta, E. A. et al. Demonstration of electron acceleration in a laser-driven dielectric microstructure. *Nature* **503**, 91–94 (2013).
54. England, R. J. et al. Dielectric laser accelerators. *Rev. Mod. Phys.* **86**, 1337–1389 (2014).
55. Keller, O. *Quantum Theory of Near-Field Electrodynamics* (Springer, 2011).
56. Linhart, J. G. Čerenkov radiation of electrons moving parallel to a dielectric boundary. *J. Appl. Phys.* **26**, 527–533 (1955).
57. Liu, H., Baskin, J. S. & Zewail, A. H. Infrared PINEM developed by diffraction in 4D UEM. *Proc. Natl Acad. Sci. USA* **113**, 2041–2046 (2016).
58. Morimoto, Y. & Baum, P. Diffraction and microscopy with attosecond electron pulse trains. *Nat. Phys.* **14**, 252–256 (2018).
59. Das, P. et al. Stimulated electron energy loss and gain in an electron microscope without a pulsed electron gun. *Ultramicroscopy* **203**, 44–51 (2019).
60. Madan, I. et al. Holographic imaging of electromagnetic fields via electron-light quantum interference. *Sci. Adv.* **5**, 8358 (2019).
61. Agostini, P., Fabre, F., Mainfray, G., Petite, G. & Rahman, N. K. Free-free transitions following six-photon ionization of xenon atoms. *Phys. Rev. Lett.* **42**, 1127–1130 (1979).
62. Corkum, P. B. & Krausz, F. Attosecond science. *Nat. Phys.* **3**, 381–387 (2007).
63. Murdia, C. et al. Controlling light emission with electron wave interference. Preprint at <https://arxiv.org/pdf/1712.04529.pdf> (2017).
64. Remez, R. et al. Observing the quantum wave nature of free electrons through spontaneous emission. *Phys. Rev. Lett.* **123**, 060401 (2019).
65. Guzzinati, G. et al. Probing the symmetry of the potential of localized surface plasmon resonances with phase-shaped electron beams. *Nat. Commun.* **8**, 14999 (2017).
66. Yang, Y. et al. Maximal spontaneous photon emission and energy loss from free electrons. *Nat. Phys.* **14**, 894–899 (2018).
67. Baum, P. & Zewail, A. H. Attosecond electron pulses for 4D diffraction and microscopy. *Proc. Natl Acad. Sci. USA* **104**, 18409 (2007).
68. Priebe, K. E. et al. Attosecond electron pulse trains and quantum state reconstruction in ultrafast transmission electron microscopy. *Nat. Photon.* **11**, 793–797 (2017).
69. Kozák, M., Schönerberger, N. & Hommelhoff, P. Ponderomotive generation and detection of attosecond free-electron pulse trains. *Phys. Rev. Lett.* **120**, 103203 (2018).
70. Kfir, O. Entanglements of electrons and cavity photons in the strong-coupling regime. *Phys. Rev. Lett.* **123**, 103602 (2019).
71. Di Giulio, V., Kociak, M. & de Abajo, F. J. G. Probing quantum optical excitations with fast electrons. *Optica* **6**, 1524–1534 (2019).

Publisher's note Springer Nature remains neutral with regard to jurisdictional claims in published maps and institutional affiliations.

© The Author(s), under exclusive licence to Springer Nature Limited 2020

Methods

Experimental set-up for the UTEM. All the experiments presented in this work were conducted using an UTEM (Jeol-2100 Plus) in nanobeam diffraction mode operating at $E_e \approx 207.2$ keV. The set-up consisted of a right-angle prism made of BK7 (index of refraction: $n = 1.512$ at $\lambda = 730$ nm) at a height of $500 \mu\text{m}$. The prism was placed on a specially designed TEM holder with one of its faces parallel to the electron beam. By splitting the laser source (LightConversion, Carbide), we created a pump–probe set-up in which one pulse is converted to an ultraviolet pulse to generate photo-electrons (probe) and the second pulse is converted to visible light, which excites the sample to create the desired electromagnetic field (pump). The probe created a coherent electron wavefunction that longitudinally extended over multiple cycles/wavelengths of the pump. Note that the coherent extent of the electron does not necessitate a pulsed excitation, as a recent paper⁵⁹ showed PINEM from electrons created in a TEM without photoexcitation.

A relative delay between the pump and probe pulses gives precise control over the relative arrival time of the electron and laser pulses, which in our experiment also describes the location of their interaction. The pump pulse (730 nm) is coupled into the prism and undergoes total internal reflection from the surface of the prism (parallel to the electron beam), exciting an evanescent near field that interacts with the electrons grazing the same surface (Fig. 2). We chose a wavelength of 730 nm, considering our optical parametric amplifier conversion efficiency, while limiting ourselves to a range where we maintained the ability to resolve individual peaks (our zero-loss peak width is ~ 1.1 eV in all figures except for Fig. 1d, where it is ~ 0.6 eV).

We used a Gatan electron energy loss spectrometer with a resolution of ~ 0.1 eV, allowing us to reveal the hidden quantum features of the interaction. The actual resolution limit for individual energy peaks is the width of the electron zero-loss peak given above. In Fig. 5, we show three examples of electron energy loss spectrometry results for the resonant phase-matched quantized electron–light interaction. We succeeded in observing electrons that gain or lose up to 300 quanta of energy with high energy resolution, identifying the individual peaks by recording several energy slices at different shifts.

To determine the correct parameters for the phase-matching, we calculated the beam path inside the prism (Supplementary Note 2a). This calculation determines the required angle of incidence of light before its transmission into the prism (40.0°), which is the prism's base angle (45.0°) minus the laser coupling angle (5.0°). This angle of incidence yields the Cherenkov angle (19.8°) of the refracted light relative to the surface of the prism for the chosen electron kinetic energy (207.2 keV) and laser wavelength (730 nm).

Grazing-angle interaction alignment challenges. The main experimental challenge of this work was the alignment of the electron beam to graze the prism's surface and to interact with the evanescent laser field near the prism surface. Any small tilt of the beam relative to the prism results in the electron beam's trajectory being pushed farther away from the surface of the prism, weakening the interaction substantially.

To achieve parallel electron illumination for a grazing-angle interaction, we chose to work in nanobeam diffraction mode with a $70\text{-}\mu\text{m}$ condenser aperture (the relatively large aperture is required because of the low current in the photo-emission mode). The current centre was then set by wobbling the objective's current (first with no condenser aperture to obtain sufficient counts) while minimizing the spot movement (spot alignment together with beam tilt). The prism tilt angle was set by minimizing the prism shadow. The condenser aperture was then inserted ($70\text{-}\mu\text{m}$ diameter) to obtain a smaller spot size, and the same steps were repeated. The estimated convergence angle of the electron beam was 1 mrad, which translates to an average distance from the prism of $x_0 \approx 500$ nm (for more details see Supplementary Note 5c).

As a final step, we minimized the deviation of the electron motion from a parallel path. The electron always follows a slightly helical path that arises from the strong magnetic field in the objective lens. We adjusted the beam tilt while looking

at the change in the prism's shadow while wobbling the objective. We estimated the helix radius and pitch using the Lorentz force $\mathbf{F} = q_e \mathbf{v}_e \times \mathbf{B}$ for our magnetic field of 1.4 T and electron convergence angle of (worst-case scenario) 1 mrad relative to the objective axis. We obtained a helical path with a pitch of 5.38 mm and radius of $0.86 \mu\text{m}$, which changed the beam distance from our prism by 100 nm. Additionally, it is important to note that, because our sample is considerably taller than regular samples, our interaction may be affected by the inhomogeneity of the magnetic field near the pole pieces.

Theoretical consideration in fitting the experiments using extended PINEM theory. We used a nonlinear optimization algorithm (Supplementary Note 5e) to fit the time delay scan data (Figs. 5c and 3a) with the theory in equation (4). The theoretical fit is presented in Figs. 5c and 3d. The fitted parameters agree well with the above experimental values (for example, of the laser spot size, laser pulse duration and so on).

Figure 4a shows that the interaction strength as a function of the acceleration voltage has multiple side lobes. These side lobes arise from the interaction being truncated by the finite length of the prism surface ($500 \mu\text{m}$). The distance between the side lobes scales inversely with this length (Supplementary Note 4 and Supplementary Fig. 4). These side lobes disappear when the transverse spatial Gaussian shape of the pump laser is considered. The laser spot size on the surface of the prism is elongated due to the angular incidence from a pump laser spot size of $100 \mu\text{m}$ to $\sim 350 \mu\text{m}$.

Data availability

All data that support the plots and other findings of this study are available from the corresponding author upon reasonable request. Source data are provided with this paper.

Acknowledgements

We thank the IDES Company and especially S.T. Park for illuminating discussions and advice. We are also grateful to I. Goykhman for fruitful discussions. The experiments were performed on the UTEM of the I. K. AdQuanta group installed in the Electron Microscopy Center (MIKA) in the Department of Material Science and Engineering at the Technion. The research was supported by ERC starting grant NanoEP 851780 and the Israel Science Foundation grant 831/19. K.W. is partially supported by a fellowship from the Lady Davis Foundation. I.K. acknowledges the support of the Azrieli Faculty Fellowship.

Author contributions

R.D. achieved the grazing-angle condition in the transmission electron microscope and led the experimental work including sample preparation. S.N. and R.D. worked on the design before the experiment began. R.D., K.W., M.S., O.B., Y.A. and S.N. carried out the experiments. K.W., S.N., Y.A., R.D., O.R. and Y.K. developed the theory and analysed the results. M.H.L. and X.S. contributed to the discussion of the results. I.K. conceived the research. All authors provided substantial input to all aspects of the project and to the writing of the manuscript.

Competing interests

The authors declare no competing interests.

Additional information

Supplementary information is available for this paper at <https://doi.org/10.1038/s41567-020-01042-w>.

Correspondence and requests for materials should be addressed to I.K.

Peer review information *Nature Physics* thanks Albert Polman and the other, anonymous, reviewer(s) for their contribution to the peer review of this work.

Reprints and permissions information is available at www.nature.com/reprints.